Repository Istituzionale dei Prodotti della Ricerca del Politecnico di Bari

On mixed-mode fracture mechanics models for contact area reduction under shear load in soft materials

(Article begins on next page)

27 April 2024

On mixed-mode fracture mechanics models for contact area reduction under shear load in soft materials

A.Papangelo$^{(a,b)}$, M. Ciavarella$^{(a,b,*)}$

$^{(a)}$*Politecnico di BARI. Center of Excellence in Computational Mechanics. Viale Japigia 182, 70126 Bari, Italy*
$^{(b)}$*Hamburg University of Technology, Department of Mechanical Engineering, Am Schwarzenberg-Campus 1, 21073 Hamburg, Germany*
**corresponding author: Mciava@poliba.it*

Abstract

The fundamental problem of friction in the presence of macroscopic adhesion, as in soft bodies, is receiving interest from many experimentalists. Since the first fracture mechanics 'purely brittle' model of Savkoor and Briggs, models have been proposed where the mixed mode toughness is interpreted with phenomenological fitting coefficients introducing weaker coupling between modes than expected by the "purely brittle" model. We compare here two such previously proposed models and introduce a third one to show that the transition to sliding is very sensitive to the form of the mixed-mode model. In particular, after a quadratic decay of the contact area with load for modest tangential loads, there could be an inflexion point and an asymptotic limit, or a jump to the Hertzian contact area. We find also that the unstable points are different under load or displacement control. The idea that the mixed mode function and parameter should be an interface property may be erroneous.

Keywords: adhesion, friction, mode-mixity, contact area shrinking, contact mechanics

1. Introduction

Adhesion and friction are two very discussed topic in tribology, and the classical Bowden-Tabor view typical for metals was that friction was largely due to adhesion, the puzzle remaining as to why adhesion could not be measured in separating the surfaces, while friction clearly was. Today the same

topics receive great attention from the academic community and large computational models are possible (Vakis et al. (2018), Pastewka & Robbins (2014)) which however do not fully answer the very fundamental open questions. In soft materials where adhesion is more evident, friction is measured also under zero closure force (Yoshizawa et al. (1993), Homola et al. (1990)), and hence a fracture mechanics model seems more promising. Indeed, Savkoor & Briggs (1977) studied the interplay of adhesion and friction for smooth spheres. They extended the JKR (Johnson et al., 1971) solution for the adhesive contact of a sphere to the case of tangential loads (see Fig. 1). However, they found that the contact area reduction was *greatly overestimated* by this "purely brittle" model in which there is an exact combination of the modes coming from Linear Elastic Fracture Mechanics theory (Fig. 1 (c)). However, there are various evidences that in many interface problems, there is an apparent increase of the toughness of the material under mixed modes, and there are various phenomenological models to interpret the mode combination effect. For example, Cao and Evans (1989) experimentally measured the material toughness for an epoxy-glass bi-material interface, showing that it strongly increases with the phase angle

$$\psi = \arctan\left(\frac{K_{II}}{K_I}\right) \tag{1}$$

being K_{II} and K_I respectively the mode II and mode I stress intensity factors. Physically, this was explained by the fact that, particularly for low crack opening, several microscopic phenomena affect the interface toughness, such as friction, plasticity and dislocation emission (Hutchinson, 1990). The simplest models include one empirical coefficient and a mode-mixity function $f(\psi)$ (Hutchinson & Suo, 1992) where the critical condition for propagation is written as

$$G = G_{Ic}f(\psi) \tag{2}$$

where G is the energy release rate, G_{Ic} is mode I critical factor (or surface energy, if we assume Griffith's concept) hence $G_{Ic}f(\psi)$ is the critical energy release rate G_c for crack propagation.

Johnson (1996) therefore reconsidered Savkoor & Briggs (1977) model introducing one such simple mode mixity function, with a quadratic dependence of the interfacial toughness on K_{II}/K_I, i.e. writing

$$f_a(\psi) = 1 + (1 - \lambda)\tan(\psi)^2 = 1 + (1 - \lambda)\left(\frac{K_{II}}{K_I}\right)^2 \qquad \text{(model "a")} \tag{3}$$

and $0 \leq \lambda \leq 1$ an empirical parameter. The case $\lambda = 0$ corresponds to the mode-uncoupling, i.e. to the rather nonphysical condition for which tangential load doesn't affect at all the adhesion process, and there is no shrinking of the contact area upon shearing. If $\lambda = 1$ instead, $f(\psi) = 1$ and this corresponds to the "ideally brittle" fracture of Savkoor & Briggs (1977) model, where frictional dissipation is neglected. The empirical constant λ permits to tune the "interaction" between modes and finds much better agreement with the area decrease with tangential load.

However, (see Fig.3 of Johnson (1996)), we also observe that, except for the limit case of the "ideally brittle" behavior ($\lambda = 1$), peeling of an adhesive contact by a tangential force occurs by a monotonically decreasing contact area with a tendency to show *an asymptotic value of reduction, and no jump instability*. For $\lambda = 1$, instead, as Savkoor & Briggs (1977) had already noticed, there is a jump instability at a critical tangential force, for which they predicted the Hertz contact radius was reached. Johnson (1996) disregarded this result because as we have discussed $\lambda = 1$ seems to be a remote limit.
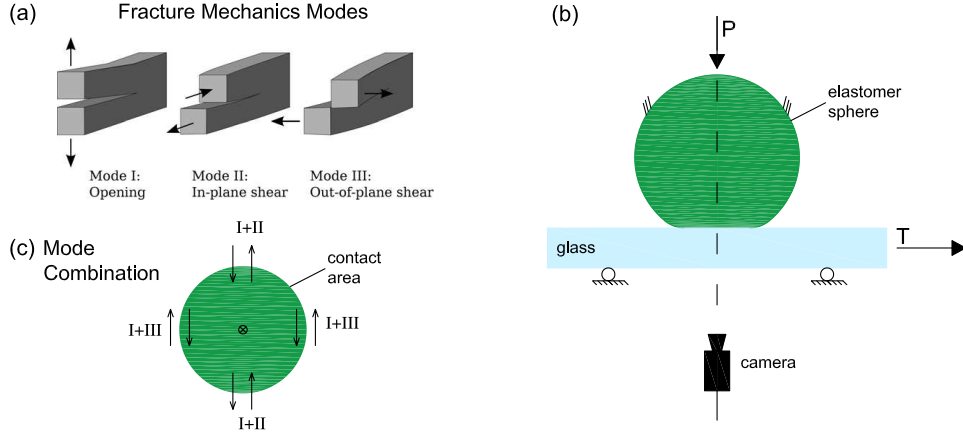

Fig. 1 - (a) Fracture mechanics modes: sketch. (b) Schematic representation of a typical experimental set-up for investigating the interplay between adhesion and friction in soft materials. Commonly, force transducers are used to measure normal and tangential loads, while a camera is used to visualize the macroscopic contact area. (c) Schematic representation of the combination of modes at the periphery of the contact area in presence of adhesion and friction

Then, Johnson (1997) tried to extend this model even further considering a more "ductile" mode of fracture, introducing a cohesive model in both mode I and mode II, where in particular he modelled the advancement of slip within the contact area, and assumed another "rather arbitrary" (as he writes) form for the interaction between modes. This resulted in possible jump instabilities only in the "ductile" regime and not in the JKR one (Johnson *et al.*, 1971), at least for the cases he considers. However, JKR equations are known to be valid even in contacts as small as those in an AFM measurements (Jacobs & Martini (2017), Ciavarella & Papangelo (2017)) and the need of the ductile model (at least, for mode I) appears rather limited. Therefore, it is worth to investigate if jump instabilities should be predicted by non-cohesive models, perhaps changing the arbitrary form of the mode mixity function.

Waters & Guduru (2010) obtained extensive experimental results of the frictional adhesive contact of a sphere on a plane surface (respectively glass on PDMS), and found that a mixed mode model like that of Hutchinson and Suo (1990)

$$f_b \left(\psi \right) = 1 + \tan^2 \left[\left(1 - \frac{\lambda}{2} \right) \psi \right] \qquad (\text{model "b"}) \qquad (4)$$

fitted results quite well[1], at least until the contact area remained circular, and beyond this case, they don't attempt further comparisons. However, beyond this level, cycles of slip instability and reattachment appeared for compressive normal loads (see Fig. 2), which should not be confused with Schallamach waves (Schallamach, 1971), but are rather single slip and reattachment events. These slip/resticking instabilities have been observed by a number of authors, but not all of them, and hence seem specific to the particular experimental testing apparatus, method and materials used (see discussion in Waters & Guduru (2010)), and one possible source of discrepancy will be given here as depending on the stiffness of the system, which could lead to situations closer to "load control" or to "displacement control". The amplitude of the tangential force oscillations is much larger for low normal loads and continuously decrease with an increase of normal load.

---

[1]Notice that for this form of Waters and Guduru (2010) mode-mixity function, λ ranges from 0 to 2. We changed the definition of λ, so that, for $\lambda \ll 1$, all the three models have the same second order expansion.
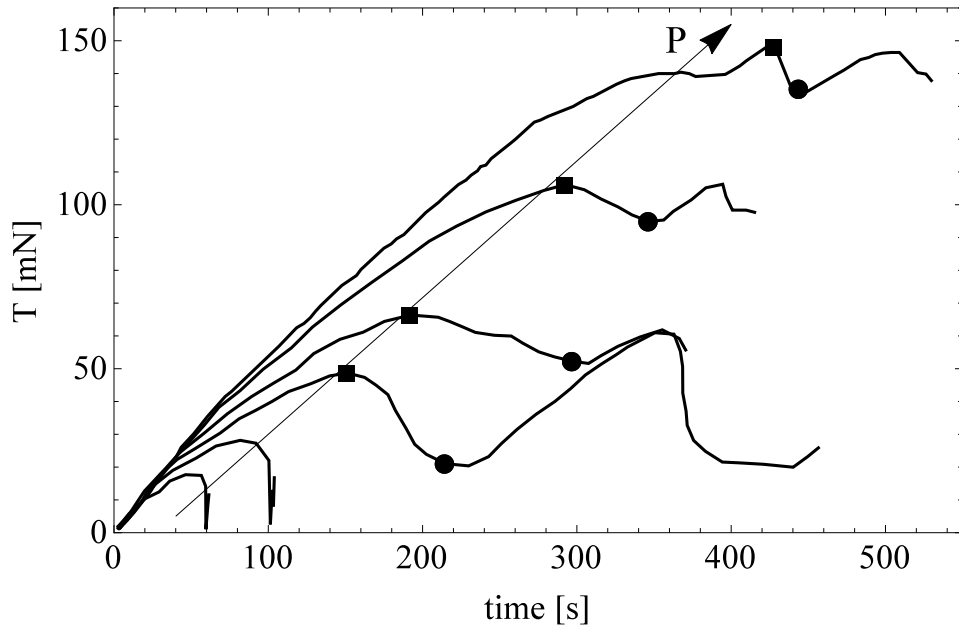
4

Fig. 2 - Loading curve: tangential load versus time for increasing normal load $P = [-5.5, -2.5, 0.5, 3.5, 9.5, 15]$ mN. Data have been extracted from Fig. 6 in Waters and Guduru (2010). Squares/circles individuate the maximum/minimum tangential force in the first cycle of detachment/reattachment.

More recently, Sahli et al. (2018) make measurements on the reduction of the contact area A upon application of shear force T for a glass-PDMS interface, suggesting a quadratic decay $A = A_0 - \alpha_A T^2$, where A_0 is the contact area at $T = 0$ and α_A is a fitting coefficient. They also find a scaling law for α_A of the form $\alpha_A \sim A_0^{-3/2}$ for both macroscopic Hertzian and rough contacts. Ciavarella (2018) has shown that qualitatively the findings of Sahli *et al.* (2018) seem justified with the mixed mode fracture mechanics model "a" but only discussed an asymptotic expansion for low reduction of contact area and small tangential load. More recently Mergel *et al.* (2018) experiments on a similar set-up report decay of the contact area which is not really quadratic for the entire range of observed behavior, as we shall discuss more in details.

It is clear that both the forms proposed by Johnson (1996) and Waters & Guduru (2010) (models "a" and "b") imply an unbounded growth of the interfacial toughness G_c under pure mode II, which has to be considered

unrealistic. Indeed, Hutchinson & Suo (1992) warn that some functional forms "should not be taken literally". Hence, in the present paper, we discuss the implications of adopting another form, also suggested by Hutchinson & Suo (1990)

$$f_c(\psi) = \left[1 + (\lambda - 1)\sin^2(\psi)\right]^{-1} \qquad (\text{model "c"}) \qquad (5)$$

which also corresponds to the very simple model

$$\frac{1}{2E^*}\left[K_I^2 + \lambda K_{II}^2\right] = G_{Ic} \qquad (6)$$

where E^* is the plain strain elastic modulus $E^* = \left(\frac{1-\nu_1^2}{E_1} + \frac{1-\nu_2^2}{E_2}\right)^{-1}$ and E_i, ν_i are the Young modulus and Poisson's ratio of the material couple. Fig. 3 shows Johnson's form f_a (dot-dashed black line), Waters-Guduru's form f_b (dashed solid line) and the proposed form f_c (red solid line), all with $\lambda = 0.15$ which is a realistically low value to produce low coupling between modes as observed in most experiments.

For $\lambda \ll 1$, the three criteria all have a quadratic form at low K_{II}/K_I, as[2]

$$f(\psi) \simeq 1 + (1 - \lambda)\psi^2 + O\left(\psi^4\right) \qquad (7)$$

and hence they start to differ at $\psi \simeq \pi/4$ or so, which is not necessarily a high value, as we shall find that the contact area has not changed much dimension in many cases at this point. Notice that (Ciavarella, 2018) explained the quadratic decay of the contact area observed in Sahli et al (2018) with Johnson's model "a", but only with some further simplifying assumptions.

It is therefore under high mode mixity that the various suggestions differ, and we shall show this has profound implications on the expected behavior of the contact, particularly on whether there is a smooth or an unstable transition to macroscopic sliding, where a high phase angle ψ is expected.

---

[2]Notice that the second order expansion of $f_b(\psi)$ is $f_b(\psi) \simeq 1 + \left(1 - \lambda + \lambda^2/4\right)\psi^2 + o(\lambda)^4$, which for $\lambda \ll 1$ reduces to $f_b(\psi) \simeq 1 + (1 - \lambda)\psi^2$.
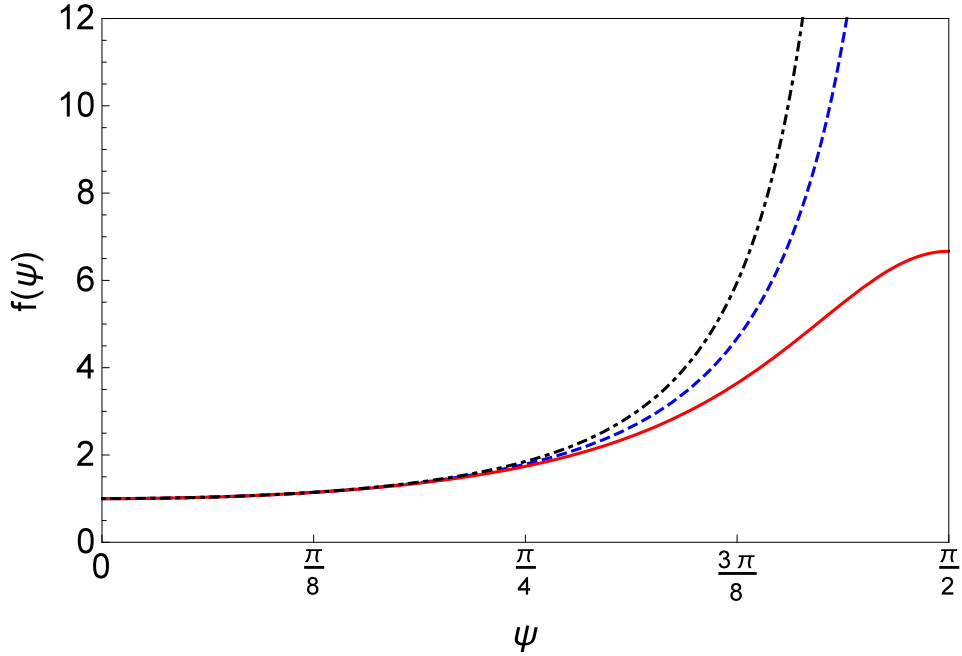
Fig. 3 - Mode mixity growth of critical strain energy release rate G_c empirical functions: Johnson's form f_a (dot-dashed black line), Waters-Guduru's form f_b (blue dashed line) and the proposed form f_c (red solid line), all with $\lambda = 0.15$ as a typical value found in experiments of Waters & Guduru (2010).

2. Fracture mechanics model

2.1. General calculations

Consider an Hertzian profile of radius R which indents an halfspace and then is sheared by a tangential force T. We assume short range adhesion at the interface, so that the JKR model (Johnson *et al.*, 1971) can be applied. This is the typical condition of most of the experiments to which we refer to, including those of Mergel et al.(2018). We assume that upon shearing, the contact area shrinks, but remains circular with radius a and no-slip enters within the contact circle, or more precisely, that the effect of slip is "included" in the form of the empirical mixed mode function: as a cohesive model describing slip like Johnson (1997) still requires an empirical mixed mode function, we find it not a very useful complication.

7

An additional difficulty in this problem arises from the fact that we have an unusual combination of modes, having all three modes of fracture present in various degrees along the interface (see Fig. 1(c)). If resistance to mode II and mode III were equal, we would actually have shrinking starting from the transverse direction, since mode III has a greater weight in the energy release rate

$$G = \frac{1}{2E^*} \left[K_I^2 + K_{II\theta}^2 + \frac{1}{1-\nu} K_{III\theta}^2 \right] \tag{8}$$

$$K_{II\theta} = \frac{T}{2a\sqrt{\pi a}} \cos(\theta); \qquad K_{III\theta} = \frac{T}{2a\sqrt{\pi a}} \sin(\theta); \tag{9}$$

(where θ is the angle between the radius vector and the direction of T and ν is the Poisson ratio) whereas the opposite is found, suggesting the strength to mode III is much higher. A detailed model requires an assumption about how to combine mode II and mode III, and there is very little evidence in the literature to do so, and anyway would result non-axisymmetric. Previous authors suggest to make an average of the mode II and mode III and this results in a Poisson's ratio coefficient corrective factor "$\frac{2-\nu}{2-2\nu}$". This small correction is inconsistent with the assumption of the axisymmetric contact area, which requires to assume that the toughness in mode III is twice higher than in mode II (assuming $\nu = 1/2$). We find more consistent to make the averaging around the periphery multiplying the mode III contribution by $1/2$, so that the energy release rate is constant along the interface and we obtain an axisymmetric failure mode, as

$$G = \frac{1}{2E^*} \left[K_I^2 + K_{II}^2 \right] \tag{10}$$

For mode I, the stress intensity factor is given by

$$K_I = \frac{P_a}{2a\sqrt{\pi a}} = \frac{P_H - P}{2a\sqrt{\pi a}} \tag{11}$$

where a is the contact radius and we have split the total load $P = P_H - P_a$ into two contributions: a compressive Hertzian load $P_H = \frac{4E^* a^3}{3R}$ and a Boussinesq flat punch solution with total load P_a which is responsible of the contact edge singularity.

In the absence of tangential force, equilibrium dictates $G = G_{Ic}$, and the standard JKR equation (10) gives the contact radius a for a given normal

8

force P

$$P = \frac{4E^*a^3}{3R} - \sqrt{8\pi E^*a^3 G_{Ic}} \qquad (12)$$

With applied tangential force T, we assume the surfaces do not slip[3], which implies a singular field of shear tractions at the interface

$$q(r) = \frac{q_0}{\sqrt{1 - \left(\frac{r}{a}\right)^2}} \qquad (13)$$

where r is the radial coordinate and $q_0 = \frac{T}{2\pi a^2}$. The distribution (13) gives rise to a uniform tangential displacement "u" within the loaded circle equal to ($\nu = 1/2$, Johnson (1985))

$$u = \frac{3\pi}{2}\frac{q_0 a}{E^*} = \frac{3}{4}\frac{T}{aE^*} \qquad (14)$$

The mode II stress intensity factor K_{II} along the shearing direction is given by

$$K_{II} = \frac{T}{2a\sqrt{\pi a}} \qquad (15)$$

Using (2) and (10), the critical condition is written as

$$\frac{1}{2E^*}\left[K_I^2 + K_{II}^2\right] = G_{Ic}f(\psi) \qquad (16)$$

which using (11) and (15) leads to

$$P = \frac{4E^*a^3}{3R} - \sqrt{8\pi E^* G_{Ic}a^3 f(\psi) - T^2} \qquad (17)$$

Equation (17) is the fundamental equation that governs the contact area reduction while the shear load is increased, for any mode mixity function $f(\psi)$.

In what follows we will adopt a dimensionless notation, as introduced by Maugis (2000)

---

[3]We have shown elsewhere (Papangelo et al. 2015) that a Coulomb frictional model involving a slip dependent friction coefficient involving microslip can lead to LEFM singular field in the limit of a small process zone. For soft materials, generally a constant shear strength is assumed in the slip zones, which corresponds to the singular mode strictly only in this limit.

$$\xi = \left(\frac{E^*R}{G_{Ic}}\right)^{1/3}; \qquad \widetilde{a} = \frac{\xi a}{R}; \qquad \widetilde{u} = \frac{u\xi^2}{R}; \qquad (18)$$

$$\widetilde{T} = \frac{T}{RG_{Ic}}; \qquad \widetilde{P} = \frac{P}{RG_{Ic}}; \qquad \widetilde{q}_0 = \frac{q_0\xi}{E^*} \qquad (19)$$

thus the JKR load-contact radius equation becomes simply

$$\widetilde{P} = \frac{4}{3}\widetilde{a}^3 - \sqrt{8\pi\widetilde{a}^3} \qquad (20)$$

and the governing equation (17) reduces to

$$\widetilde{P} = \frac{4}{3}\widetilde{a}^3 - \sqrt{8\pi\widetilde{a}^3 f\left(\psi\right) - \widetilde{T}^2} \qquad (21)$$

Using eq. (3,4,5) into (21), the governing equations for the three models considered are obtained, in particular, as

- Johnson's model (model "a")

$$\widetilde{P} = \frac{4}{3}\widetilde{a}^3 - \sqrt{8\pi\widetilde{a}^3 \left[1 + (1-\lambda)\frac{\widetilde{T}^2}{\left(\frac{4}{3}\widetilde{a}^3 - \widetilde{P}\right)^2}\right] - \widetilde{T}^2} \qquad (22)$$

- Waters and Guduru's model (model "b")

$$\widetilde{P} = \frac{4}{3}\widetilde{a}^3 - \sqrt{8\pi\widetilde{a}^3 \left\{1 + \tan^2\left[\left(1 - \frac{\lambda}{2}\right)\arctan\left(\frac{\widetilde{T}}{\frac{4}{3}\widetilde{a}^3 - \widetilde{P}}\right)\right]\right\} - \widetilde{T}^2} \qquad (23)$$

- proposed model (model "c"), which turns out to have also the simplest form

$$\widetilde{P} = \frac{4}{3}\widetilde{a}^3 - \sqrt{8\pi\widetilde{a}^3 - \lambda\widetilde{T}^2} \qquad (24)$$

We first plot results in the form of contact radius vs normal load curves for various tangential loads $\widetilde{T} = [10, 20, 30, 40]$ for Fig. 4 (a,c), $\widetilde{T} = [10, 40, 70, 100]$

10

for Fig. 4 (b) and $\lambda = 0.15$ as a representative value permitting weak coupling between modes — the single value obviously fits the same data only at low K_{II}/K_I values, see Fig. 3. All curves in Fig. 4 (a-b-c correspond to model a,b,c respectively) lie in between the JKR (dot-dashed) and Hertz (dashed) known limits. However, the detailed form of the mixed mode functions varies significantly the response, particularly in the way the solution remains similar to JKR, with just a smooth but small reduction of the contact area as in models a and b, or tends to Hertz with an unstable point. If the unstable point is in the tensile region, obviously this predicts a jump off contact, whereas in cases when this occurs in the area of compressive loads, we would expect a jump to Hertz contact. We notice in particular the following features:

- Johnson (1996) model "a" (Fig. 4 (a)) shows virtually only one possible detachment instability at negative loads, very close to the JKR pull-off, and the curve contact radius vs normal load, increasing the tangential load, rapidly converges to a limit curve. There is therefore no jump instability in the compressive region[4];

- Waters-Guduru model "b" (Fig. 4 (b)) shows a jump instability, which persists to some extent also for compressive loads and then becomes a smooth transition into Hertz regime;

- The "proposed" model "c"(Fig. 4 (c)) shows a more marked jump instability which is present for *all* values of normal load. For tensile loads, at the jump instability point, detachment occurs (jump off contact). For compressive loads, at the jump instability point, the contact area drops in size to the Hertzian value;

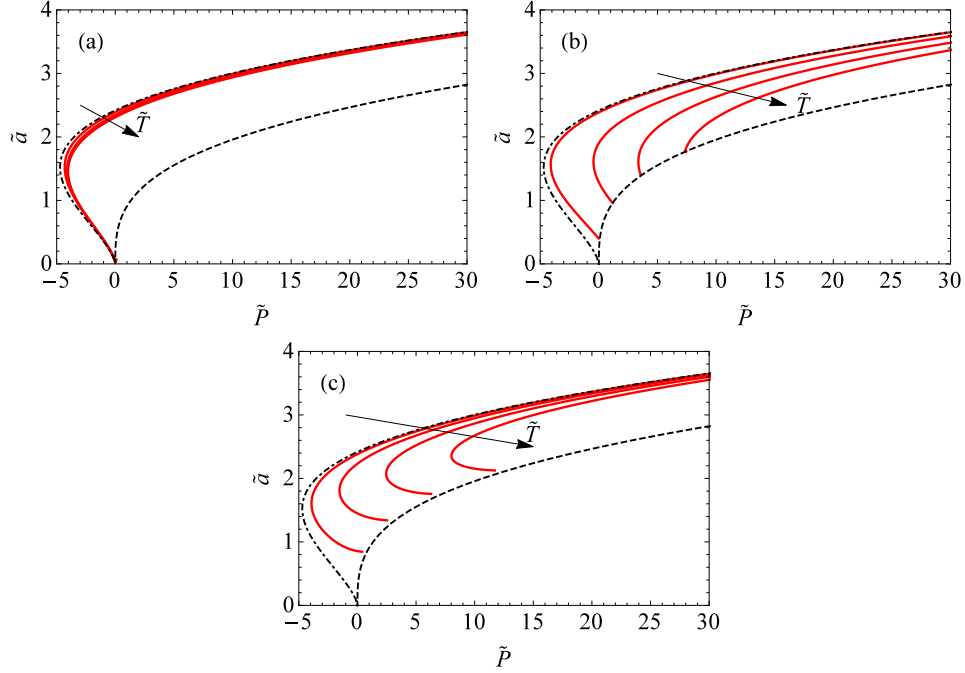[4]Except for the limit case of $\lambda = 1$

Fig. 4 - Contact radius as a function of normal load for $\lambda = 0.15$ and $\widetilde{T} = [10, 20, 30, 40]$ for (a,c) while $\widetilde{T} = [10, 40, 70, 100]$ for (b). All curves develop between JKR (dot-dashed) and Hertz (dashed) curves for (a) Johnson (1996) model (b) Waters-Guduru model (c) proposed model.

In Fig. 5 the possible qualitative behaviors are summarized. Starting at zero tangential load, the solution corresponds to that of JKR (Johnson *et al.*, 1971). Upon shearing the contact area shrinks:

1. continuously up to a non Hertzian solution (Fig. 5, label (1));
2. continuously up to the Hertzian solution (Fig. 5, label (2));
3. continuously up to critical value and then it drops suddenly up to the Hertzian value (Fig. 5, label (3));

Notice that some authors (Mergel *et al.*, 2018) have suggested that full-sliding takes place upon reaching a critical interfacial shear strength τ_0 (a property of the interface) (Fig. 5, label (4)), thus we keep the conservative view to consider two competing mechanisms: fracture mechanics ones described in (1-2-3) and the shear-strength criterion $T_{full} = \tau_0 A$ (Fig. 5, label (4)).
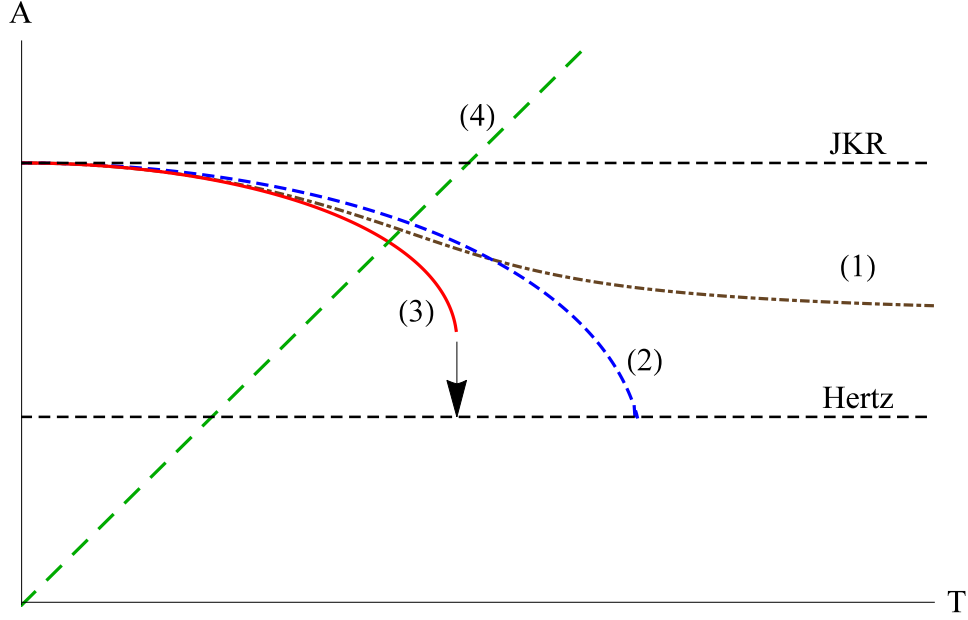
Fig. 5 - Contact area vs tangential load. The possible qualitative behaviors are plotted and labeled with (1-3). In particular, upon shearing the contact area may shrink continuously up to a non Hertzian solution (1), continuously up the the Hertzian solution (2), continuously up to a critical point and then with a jump instability up to the Hertzian solution (3). Some authors have proposed that full sliding happens when a critical shearing traction is reached at the interface $\tau_0 = T_{full}/A$ (4).

2.2. Loading curves

For given normal load $\widetilde{P}$ we look for the equilibrium relation between the tangential load $\widetilde{T}$ and the uniform tangential displacement $\widetilde{u}$. Substituting eq. (14) into (24), after some algebra, the relation $\widetilde{u}\left(\widetilde{T}\right)$ is obtained analytically (for model "c")

$$\widetilde{u} = \frac{3^{2/3}}{2}\left(\frac{3\pi + \widetilde{P} \pm \sqrt{9\pi^2 - \lambda\widetilde{T}^2 + 6\pi\widetilde{P}}}{2\lambda\widetilde{T}^2 + 2\widetilde{P}^2}\right)^{1/3}\widetilde{T} \qquad (25)$$

where we left a "$\pm$" sign, which indicates two different branches.

(a)

$\tilde{u}$

$\tilde{T}$

$\tilde{P}$

(b)

$\tilde{A}$

$\tilde{T}$

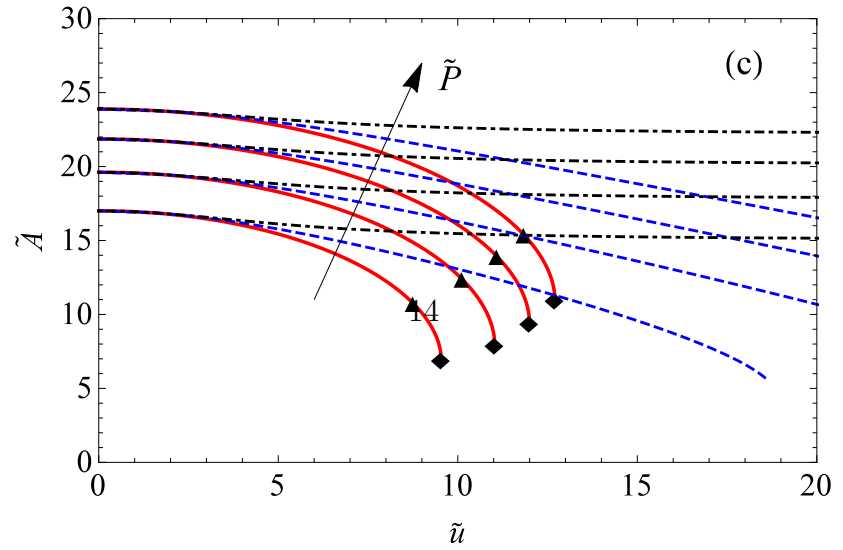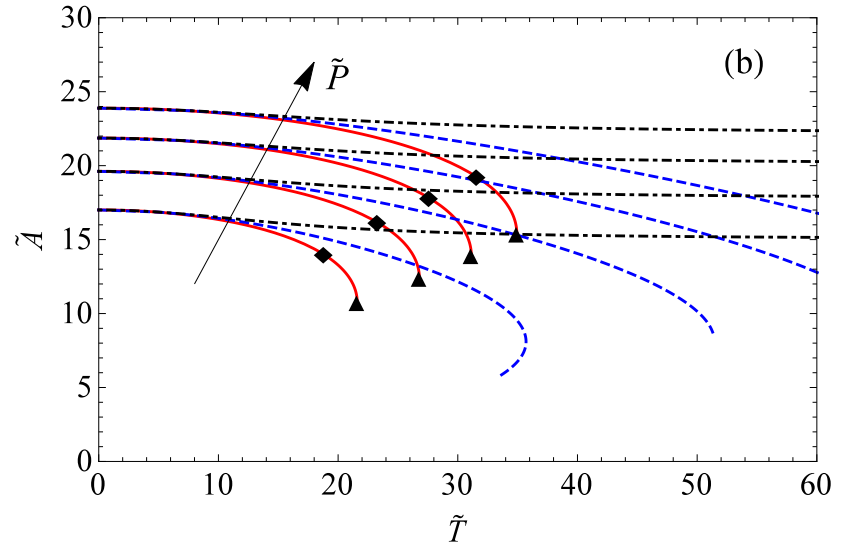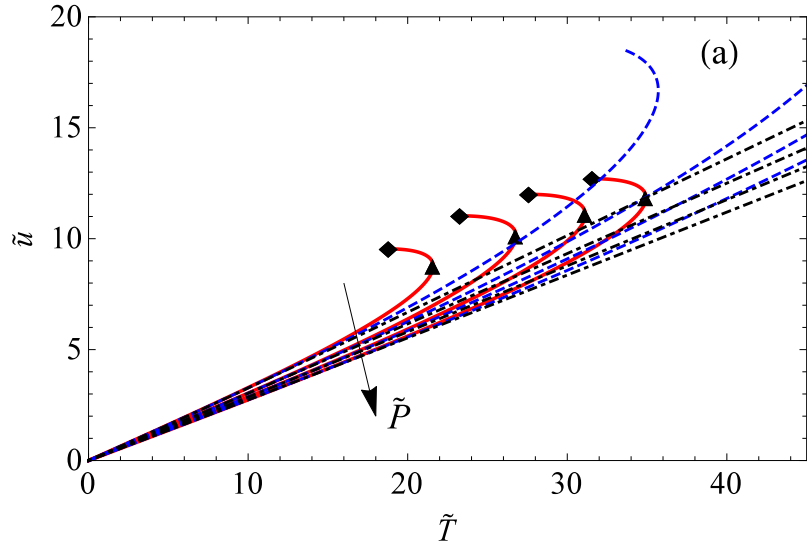$\tilde{P}$

(c)

$\tilde{A}$

$\tilde{u}$

$\tilde{P}$

14

Fig. 6 - (a) Tangential displacement vs tangential load, (b) contact area vs tangential load and (c) contact area vs tangential displacement for $\widetilde{P} = [-1, 1, 3, 5]$ and $\lambda = 0.15$. In all panels black dot-dashed line for model "a" Johnson (1996), blue dashed line for model "b" Waters-Guduru (2010) and red solid line for the proposed model "c". For the proposed model "c", the instability points under load (triangles) and displacement (diamonds) control are indicated.

In Fig. 6 the loading curves (panel (a) $\widetilde{u}$ vs $\widetilde{T}$, panel (b) $\widetilde{A}$ vs $\widetilde{T}$, panel (c) $\widetilde{A}$ vs $\widetilde{u}$) are plotted using $\widetilde{P} = [-1, 1, 3, 5]$ and $\lambda = 0.15$ for the three models considered: Johnson model "a" (black dot-dashed line), Waters-Guduru model "b" (blue dashed line) and proposed model "c" (red solid line). Notice that only the physically meaningful branches have been drawn. In Fig. 6 (a) the equilibrium relation $\widetilde{u}\left(\widetilde{T}\right)$ is plotted. While for the model "c" we have derived the relation $\widetilde{u}\left(\widetilde{T}\right)$ analytically (25), for the two models "a" and "b" the curves have been obtained numerically using eq. (14) and (24). Immediately one notice that the three models behave very differently. In particular for the Johnson model $\widetilde{u}\left(\widetilde{T}\right)$ may be well approximated by a linear relation, for Waters-Guduru model the curve $\widetilde{u}\left(\widetilde{T}\right)$ starts to bend nonlinearly, and the proposed model "c" shows two marked instability points, one under load (triangle symbols), and the other under displacement control (diamond symbols).

Fig. 6 (b-c) plots the contact area $\widetilde{A} = \pi\widetilde{a}^2$ vs tangential load $\widetilde{T}$ and displacement $\widetilde{u}$. Fig. 6 (b-c) shows that Johnson (1996) model "a" is almost insensitive to the tangential load (displacement) with this value of λ: this is because the toughness grows already very significantly (see Fig. 3). This explains why we did find $\widetilde{u}$ to have almost a linear dependence on $\widetilde{T}$. At the other extreme, with the proposed model "c" , the area decays in a quasi-elliptical fashion and shows the marked jump instability we have already discussed at a critical value of the tangential load (Fig. 6 (b-c)). An intermediate behavior is shown by the Waters-Guduru model.

Solving in particular eq. (24) for $\widetilde{a}$, the contact area $\widetilde{A}$ is found as

$$\widetilde{A} = \pi \left(\frac{3}{4}\right)^{2/3} \left[3\pi + \widetilde{P} \pm \sqrt{9\pi^2 + 6\pi\widetilde{P} - \lambda\widetilde{T}^2}\right]^{2/3} \tag{26}$$

where the "±" indicates two possible branches[5]. Sahli *et al.* (2018) suggested a quadratic decay for the contact area with the tangential load $\widetilde{A} = \widetilde{A}_0 - \widetilde{\alpha}_A \widetilde{T}^2$ (where $\widetilde{A}_0$ is the dimensionless contact area for null tangential load and $\widetilde{\alpha}_A = \alpha_A \xi^2 G_{Ic}^2$ is a fitting parameter) and in view of the fact that all models are similar at low tangential load, we could expand in series eq. (26) up to the second order to find an analytical expression for $\widetilde{\alpha}_A$. This gives

$$\widetilde{\alpha}_A = \frac{\lambda}{6 \times 3^{2/3} \, (2\pi)^{1/3} \, \sqrt{1 + \frac{2\widetilde{P}}{3\pi}} \left(1 + \frac{\widetilde{P}}{3\pi} + \sqrt{1 + \frac{2\widetilde{P}}{3\pi}} \right)^{1/3}} \tag{27}$$

Sahli et al. (2018) showed a scaling law for α_A with respect to the contact area for null tangential load A_0, over four orders of magnitude. Using $\widetilde{P} = \frac{4}{3} \left(\frac{\widetilde{A}_0}{\pi} \right)^{3/2} - \sqrt{8\pi} \left(\frac{\widetilde{A}_0}{\pi} \right)^{3/4}$, eq. (27) is rewritten as

$$\widetilde{\alpha}_A = \frac{\pi^{7/4} \lambda}{2 \times 2^{1/3} g\left(\widetilde{A}_0 \right) \left[4\widetilde{A}_0^{3/2} + 3\pi^{5/4} \left(3\pi^{5/4} - 2\sqrt{2} \widetilde{A}_0^{3/4} + g\left(\widetilde{A}_0 \right) \right) \right]^{1/3}} \tag{28}$$

where $g\left(\widetilde{A}_0 \right) = \sqrt{8\widetilde{A}_0^{3/2} - 12\sqrt{2}\pi^{5/4}\widetilde{A}_0^{3/4} + 9\pi^{5/2}}$. In the limit of high $\widetilde{A}_0$

$$\widetilde{\alpha}_A \simeq \frac{\pi^{7/4} \lambda}{8\sqrt{2}} \widetilde{A}_0^{-5/4} \tag{29}$$

which predicts a power law decay with exponent $-5/4$ which agrees with Ciavarella (2018) and is close to $-3/2$ found by Sahli et al. (2018) in their experiments.

We can also obtain exact results for the jump instability points in the proposed model "c". Under displacement control, at the jump instability point (diamonds in Fig. 6), the derivative of the tangential displacement with respect to the tangential load $\frac{d\widetilde{u}}{d\widetilde{T}}$ vanishes, thus the critical tangential load $\widetilde{T}_u$, tangential displacement $\widetilde{u}_u$ and contact area $\widetilde{A}_u$ at the jump instability points under displacement control are obtained

---

[5]In Fig. 6 we drew only the physically meaningful branches.

16

$$\widetilde{T}_u = \frac{1}{2}\sqrt{\frac{3}{2}\frac{9\pi^2 + 6\pi\widetilde{P} - 3\widetilde{P}^2 + \sqrt{3\left(3\pi + \widetilde{P}\right)^2\left(3\pi^2 + 2\pi\widetilde{P} + 3\widetilde{P}^2\right)}}{\lambda}} \qquad (30)$$

$$\widetilde{u}_u = \left(\frac{3}{4}\right)^{2/3}\frac{\widetilde{T}_u}{\left(3\pi + \widetilde{P} + \sqrt{9\pi^2 + 6\pi\widetilde{P} - \lambda\widetilde{T}_u^2}\right)^{1/3}} \qquad (31)$$

$$\widetilde{A}_u = \pi\left(\frac{3}{4}\right)^{2/3}\left[3\pi + \widetilde{P} \pm \sqrt{9\pi^2 + 6\pi\widetilde{P} - \lambda\widetilde{T}_u^2}\right]^{2/3} \qquad (32)$$

Under load control, at the jump instability point (triangles in Fig. 6), the derivative of the contact area with respect to the tangential load $\frac{d\widetilde{A}}{d\widetilde{T}}$ is singular, thus the critical tangential load $\widetilde{T}_T$, tangential displacement $\widetilde{u}_T$ and contact area $\widetilde{A}_T$ at the jump instability points under load control are obtained

$$\widetilde{T}_T = \sqrt{\frac{3\pi\left(3\pi + 2\widetilde{P}\right)}{\lambda}} \qquad (33)$$

$$\widetilde{u}_T = \left[\frac{(3/4)^2}{3\pi + \widetilde{P}}\right]^{1/3}\sqrt{\frac{3\pi\left(3\pi + 2\widetilde{P}\right)}{\lambda}} \qquad (34)$$

$$\widetilde{A}_T = \pi\left(\frac{3}{4}\right)^{2/3}\left(\frac{3}{2}\pi + \lambda\frac{\widetilde{T}_T^2}{6\pi}\right)^{2/3} \qquad (35)$$

From eq. (35), for $\widetilde{T}_T \gg 3\pi/\sqrt{\lambda}$, the critical tangential load scales as $\widetilde{T}_T \to \left(\frac{\widetilde{A}_T}{0.37\lambda^{2/3}}\right)^{3/4}$ which is close to the linear increase of the alternative criterion of full sliding proposed, for example, by Sahli et $al.$ (2018) and Mergel et $al.$ (2018) $\widetilde{T}_{full} = \widetilde{\tau}_0\widetilde{A}$, where $\widetilde{\tau}_0 = \tau_0\xi/E^*$ is an interfacial property. Whether the jump instability really occurs or not may not be a trivial question to answer experimentally, and obviously may depend on the particular experimental conditions and specific material. As we have also obtained that the jump instabilities depend on the stiffness of the system (with load control being

17

valid in the limit of soft loading setup and displacement control for very stiff loading setup), this is also a possible explanation of the disagreement over the occurrence of the cycles of slip and reattachment cycles reported by some but not all authors (see the discussion in the paper of Waters-Guduru (2010)).

Also, from Fig. 4 we conclude that the jump instability will appear at most only at low normal loads, and then it should disappear for two reasons: one is the absence of the jump instability point in many mixed mode models, and the other is that, for high normal loads, Hertz contact area will be close anyway to the area with adhesion (the leading term in eq. (20) is the adhesionless one "$\widetilde{a}^3$"). This is in agreement with the observation of Waters-Guduru (2010), who observed in their Fig. 6 that the jump instability reduces increasing the normal load (see Fig. 1).

3. Detailed comparison with experimental results

We discuss some comparisons of the models predictions with the experimental results published by Mergel *et al.* (2018, their Fig. 5 (c)). From Mergel *et al.* (2018) the following parameters can be extracted: $G_{Ic} = 27$ mJ/m^2, $R = 9.42$ mm, $E^* = 2.133$ MPa. To assess the mode mixity function, we use the fracture mechanics model rewritten in the form

$$\frac{G_c}{G_{Ic}} = f\left(\psi\right) = \frac{\left(\frac{4E^*a^3}{3R} - P\right)^2 + T^2}{8\pi E^* a^3 G_{Ic}} \tag{36}$$

so that the ratio G_c/G_{Ic} as a function of ψ can be obtained directly from the experiments (Fig. 7, gray symbols) and compared with the proposed model (solid red line), Waters & Guduru (dashed blue line) and Johnson (1966) (dot-dashed black line). The extremely low value of $\lambda = 0.0023$ (coefficient of determination $R^2 = 0.9999$) has been obtained using a least-square best fit procedure of the proposed model $f_c\left(\psi\right)$, using the data in the form $\log\left(\frac{G_c}{G_{Ic}}\right)$ vs ψ. We assume the same λ holds for the other two criteria since they have the same form to the second order.
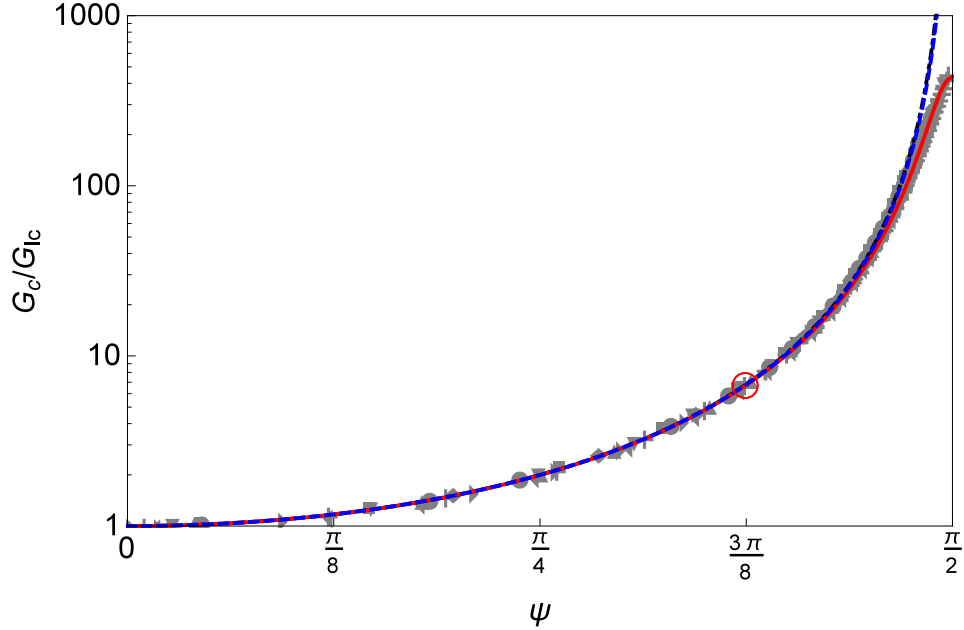
Fig. 7 - G_c/G_{Ic} is plotted for the experimental data (gray symbols) in Mergel *et al.* (2018, their Fig. 5 (c)). The dot-dashed, dashed, solid lines stand respectively for the Johnson (1966) model "a", Waters & Guduru model "b", proposed model "c". Notice that the models "a" and "b", respectively dot-dashed and dashed lines, are superposed and almost indistinguishable. The values of $\lambda = 0.0023$ and the coefficient of determination $R^2 = 0.9999$ has been obtained using a least-square best fit procedure of the proposed model $f_c(\psi)$ using the data in the form $\log\left(\frac{G_c}{G_{Ic}}\right)$ vs ψ. We assume the same λ holds for the other two criteria since they have the same form to the second order.

The best results have been obtained with the suggested model $f_c(\psi)$. However, this is not so evident in the energy release rate fit, as it is from the contact area predictions in Fig 8. With the fitted λ we directly compare the experimental area vs tangential load curves with the analytical predictions respectively for (a) Johnson (1996) model (b) Waters-Guduru model and (c) proposed model. It is clearly shown that the suggested mode-mixity function $f_c(\psi)$ fits the experimental data of Mergel *et al.* (2018) much better than the Johnson (1966) and Waters & Guduru (2010) model. Notice that the poor fit of the latter models "a" and "b" is not due to our choice of a single λ - we have attempted to tune λ to best fit the data in the entire range but

19

this resulted always in a poor fitting, with low coefficient of determination. Instead, with the model "c", the decay is better fitted in a much wider range, some discrepancies arising only very close to the jump instability point. In all the panels (a, b, c) we have highlighted with a red circle the point which corresponds to $\psi = \frac{3\pi}{8}$ and the same red circle is shown in Fig. 7, to show that most of the experimental points lie in the region of high ψ, where the three models presented differ considerably.

Fig. 8 (c) shows a dot-dashed line for the full sliding criterion $T_{full} = \tau_0 A$, with $\tau_0 = 0.43$ MPa (the value reported by Mergel *et al.* (2018)), while the dashed line stands for eq. (35). It is clear that the two criteria are almost indistinguishable in Mergel *et al.* (2018) experimental conditions, so that it is not safe to make a statement as to which criterion is met. Mergel *et al.* (2018) conclude for the strength based criterion, but we find this not so obvious.
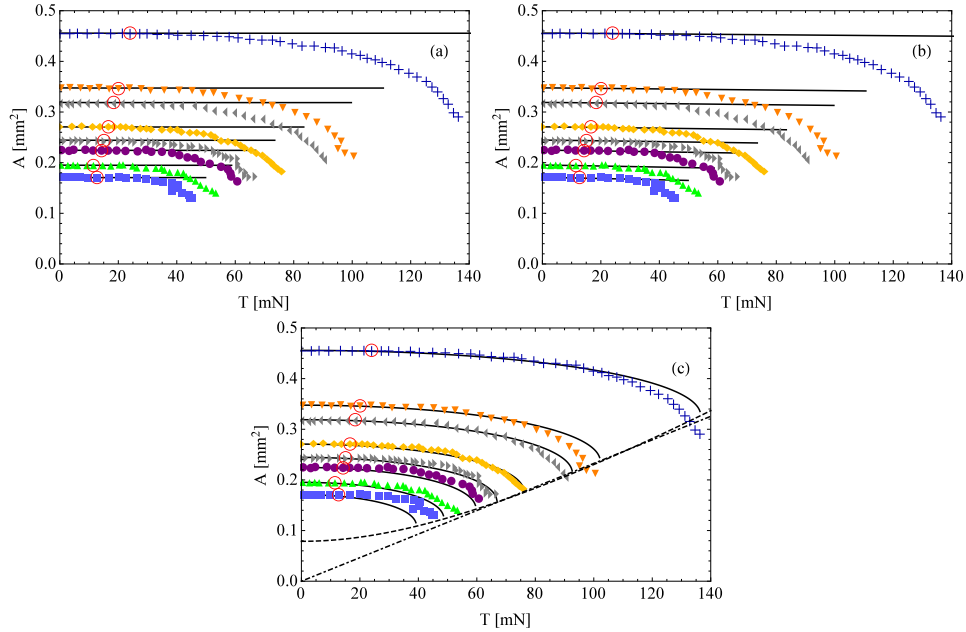

Fig. 8 - Contact area as a function of tangential load for the curves with normal load $\widetilde{P} = [30.4, 15.0, 11.5, 6.2, 3.7, 2.0, -0.23, -1.79]$ using $\lambda = 0.0023$ for (a) Johnson (1996) model (b) Waters-Guduru model and (c) proposed model. Solid lines are the theoretical predictions while colored symbols stand for the experimental results (from Mergel *et al.* (2018), their Fig. 5 (c)). In all the panels (a, b, c) the points corresponding to $\psi = \frac{3\pi}{8}$ are highlighted with a red circle. The same red circle is shown in Fig. 7. In

20

panel (c) dot-dashed line stands for $T_{full} = \tau_0 A$ ($\tau_0 = 0.43$ MPa, as reported in Mergel *et al.* (2018)) while dashed line stands for eq. (35).

We then move to discuss the original data of Waters and Guduru (2010), which unfortunately were reported only for initial decay of the contact area, where they observed a strictly axisymmetric configuration. Fitting the mode mixity function, we find no evidence that our proposed model "c" should be any better than their model "b". Our best fit gives for the model "c" $\lambda = 0.2331$, while for Waters-Guduru model we confirm the same $\lambda = 0.30$ which they suggest[6]. Notice that here we only have data up to $f(\psi) \approx 3$ and mode mixity angle of $3/8\pi$, so the comparison of the models ends much earlier than in the previous comparison with experimental data (see Fig. 9). It is however in the comparison of the contact area decay with tangential load where some (possible) improvement emerges (Fig. 10). Clearly, the data show a much better overall agreement with the model.
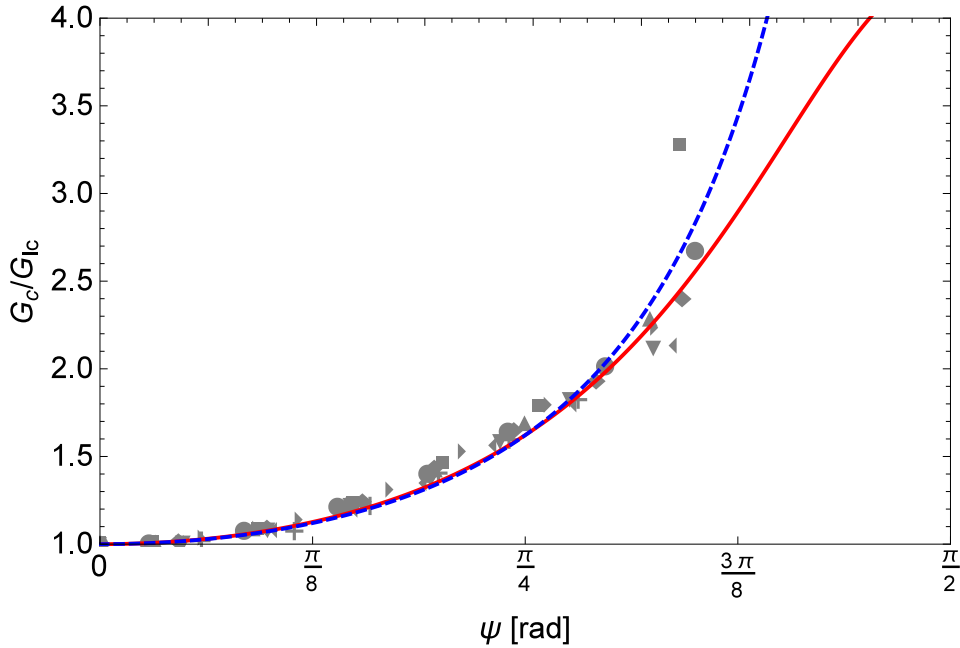

Fig. 9 - G_c/G_{Ic} is plotted for the experimental data (gray symbols) in Waters and Guduru (2010) (data extracted from their Fig. 8). The best fit

---

[6]Notice that our definition of λ is twice the λ in Waters and Guduru (2010) paper.

procedure provided $\lambda = 0.2331$ for the model (c) (solid line). For Waters and Guduru model "b" (dashed line) we used their fit $\lambda = 0.30$ (notice that our definition of λ is twice the λ in Waters and Guduru (2010) paper).
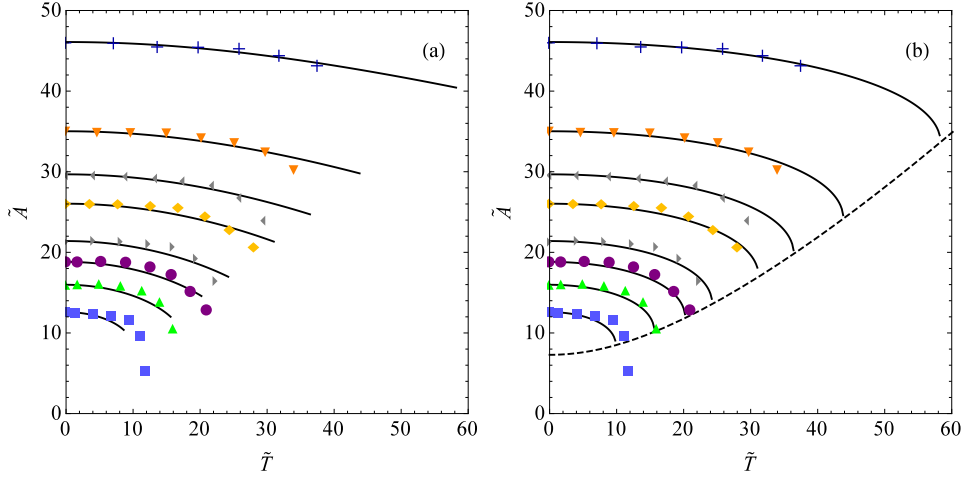

Fig. 10 - Contact area as a function of tangential load for Waters and Guduru (2010) data (their Fig. 8) in dimensionless form. (a) model "b" by Waters and Guduru, (b) our proposed model "c".

As a way to investigate if the jump instabilities we predict in our model are related to the cycles of detachment/reattachment in Waters-Guduru (2010), in the absence of better data (the authors report mostly results at moderate loads because of their choice of plotting only axisymmetric results), we plot in Fig. 11 the ratio between tangential force T and the Hertz contact area A_H at the given value of normal load, which we could gather from their Fig. 6 (here reproduced as our Fig. 1). For the tangential force, we used two set of data: the maximum (squares in Fig. 1) and minimum (circles in Fig. 1) tangential forces in the first cycle of detachment/reattachment. Accordingly with our previous analysis, the minima of tangential loads should correspond to full-sliding solution with a Hertzian value of contact area, which, in turns, should approximately correspond along with a "material constant" shear strength τ_0, as it is often measured for soft materials. Fig. 11 shows indeed that the value obtained for the average shear stress is nearly constant, whereas the same hypothesis does not work for the points at the maxima of tangential load. Indeed for low normal load the data suggest more an unstable jump

rather than a smooth transition to full sliding in accordance to the proposed model "c".
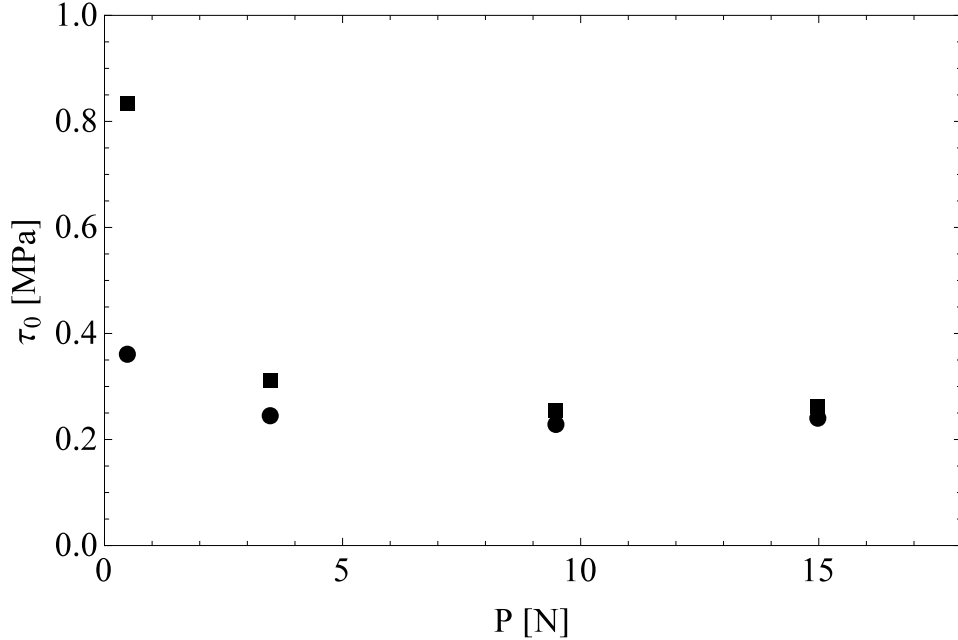

Fig. 11 - Average shear stress computed as tangential force divided by Hertzian contact area as a function of normal load in Waters and Guduru (2010) data (data extracted from their Fig. 6, our Fig. 1). Squares refer to the maximum tangential forces (corresponding to the squares in Fig. 1), circles to the minimum tangential forces (corresponding to the circles in Fig. 1) in the first cycle of detachment/reattachment.

4. Conclusions

In this work, we have discussed the implications of adopting different mode-mixity functions to account for the dependence of the interfacial toughness on the phase angle $\psi = \arctan\left(\frac{K_{II}}{K_I}\right)$ in an adhesive contact subjected to tangential load. Three different models have been compared, all originally proposed by Hutchinson & Suo (1992) in the framework of fracture mechanics of bi-material interfaces, but of which only two have been used so far, respectively by Johnson (1996) and Waters & Guduru (2010) in the particular problem of contact area shrinking under shear loads. We showed

23

that changing the mode-mixity function different contact behaviors can be obtained, particularly for high phase angles $\psi > 3\pi/8$, values that are quite common in the experiments reported in the literature (Waters & Guduru (2010), Mergel *et al.* (2018)). It was shown that, depending on the interfacial properties, smooth shrinking of contact area up to full sliding or abrupt drop to the Hertzian solution through a jump instability may be observed which depends on the type of load control.

Neither Johnson (1966) nor Waters & Guduru (2010) models fit Mergel *et al.* (2018) experimental results accurately, because the contact area remains almost constant for moderate loads. The model we propose fits reasonably well the data, and the locus of the jump instability points turns out to be extremely close to the strength criterion condition $\widetilde{T}_{full} = \widetilde{\tau}_0 \widetilde{A}$ suggested by Mergel *et al.* (2018). In the data of Waters & Guduru (2010), our model seems to lead more naturally to the jump instability points, and the average shear stress $\widetilde{\tau}_0$ at the minima of tangential load seem to be indeed a "material constant", as it is usually observed for soft materials. More investigations are needed to ascertain which conditions are to be expected in the transition to sliding of soft materials, but it is clear that the influence of the mixed mode function at high mode mixity is crucial.

Author Contribution Statement

AP and MC contributed equally to this work.

Acknowledgements

References

Cao, H. C., & Evans, A. G. (1989). An experimental study of the fracture resistance of bimaterial interfaces. Mechanics of materials, 7(4), 295-304.

Ciavarella, M. (2018). Fracture mechanics simple calculations to explain small reduction of the real contact area under shear. Facta universitatis, series: mechanical engineering, 16(1), 87-91.

Ciavarella, M., & Papangelo, A. (2017). Discussion of "Measuring and Understanding Contact Area at the Nanoscale: A Review"(Jacobs, TDB,

and Ashlie Martini, A., 2017, ASME Appl. Mech. Rev., 69 (6), p. 060802). Applied Mechanics Reviews, 69(6), 065502.

Homola, A. M., Israelachvili, J. N., McGuiggan, P. M., & Gee, M. L. (1990). Fundamental experimental studies in tribology: The transition from "interfacial" friction of undamaged molecularly smooth surfaces to "normal" friction with wear. Wear, 136(1), 65-83.

Hutchinson, J. W. (1990). Mixed mode fracture mechanics of interfaces. Metal-ceramic interfaces, 4, 295-306.

Hutchinson, J. W. & Suo, Z. (1992). Mixed mode cracking in layered materials. In Advances in applied mechanics, vol. 29 (eds J. W. Hutchinson & T. Y. Wu), pp. 63–191. Boston, MA: Academic Press.

Jacobs, T. D. B., & Martini, A. (2017). Measuring and understanding contact area at the nanoscale: a review. Applied Mechanics Reviews, 69(6), 060802.

Johnson, K. L., Kendall, K. & Roberts, A. D. (1971) Surface energy and the contact of elastic solids. Proc. R. Soc. Lond. A 324, 301–313.

Johnson, K. (1985). Contact Mechanics. Cambridge: Cambridge University Press. doi:10.1017/CBO9781139171731

Johnson, K. L., (1997), Adhesion and friction between a smooth elastic spherical asperity and a plane surface. In Proceedings of the Royal Society of London A453, No. 1956, pp. 163-179).

Johnson KL, (1996), Continuum mechanics modeling of adhesion and friction. Langmuir 12:4510–4513.

Maugis, D. (2013). Contact, adhesion and rupture of elastic solids (Vol. 130). Springer Science & Business Media.

Mergel, J. C., Sahli, R., Scheibert, J., & Sauer, R. A. (2018). Continuum contact models for coupled adhesion and friction. The Journal of Adhesion, DOI: 10.1080/00218464.2018.1479258

Papangelo, A., Ciavarella, M., & Barber, J. R. (2015). Fracture mechanics implications for apparent static friction coefficient in contact problems involving slip-weakening laws. Proc. R. Soc. A, 471(2180), 20150271.

Pastewka, L., & Robbins, M. O. (2014). Contact between rough surfaces and a criterion for macroscopic adhesion. Proceedings of the National Academy of Sciences, 201320846.

Sahli, R., Pallares, G., Ducottet, C., Ben Ali, I. E., Al Akhrass, S., Guibert, M., Scheibert, J. (2018). Evolution of real contact area under shear, Proceedings of the National Academy of Sciences, 115 (3) 471-476; DOI: 10.1073/pnas.1706434115

Savkoor, A. R. & Briggs, G. A. D. (1977). The effect of a tangential force on the contact of elastic solids in adhesion. Proc. R. Soc. Lond. A 356, 103–114.

Schallamach, A. (1971). How does rubber slide?. Wear, 17(4), 301-312.

Vakis, A. I., Yastrebov, V. A., Scheibert, J., Minfray, C., Nicola, L., Dini, D., ... & Molinari, J. F. (2018). Modeling and simulation in tribology across scales: An overview. Tribology International 125, 169-199. DOI: 10.1016/j.triboint.2018.02.005

Waters JF, Guduru PR, (2010), Mode-mixity-dependent adhesive contact of a sphere on a plane surface. Proc R Soc A 466:1303–1325.

Yoshizawa, H., Chen, Y. L., & Israelachvili, J. (1993). Fundamental mechanisms of interfacial friction. 1. Relation between adhesion and friction. The Journal of Physical Chemistry, 97(16), 4128-4140.